Effect of the tip structure on atomic-force microscopy

Naruo Sasaki and Masaru Tsukada
Department of Physics, University of Tokyo, Hongo 7-3-1, Bunkyo-ku, Tokyo 113, Japan
and JRDC, Pre-Research Program Laboratory, Ikenohata 1-1-15, Taitoh-ku, Tokyo 110, Japan
(Received 20 March 1995)

Theoretical simulation of atomic-force microscope (AFM) images is performed with a model of a single-atom tip or two kinds of multiple-atom diamond tips scanned on a graphite substrate surface. Several fundamental effects on AFM images are systematically investigated. First, it is made clear how the AFM images and the force distributions change as the load varies. Then, for the multiple-atom tips, the effects of the tip orientation and the tip apex structure, including the bond length, are examined. The characteristics of the AFM images, such as their detailed microscopic pattern, the symmetry, and the corrugation amplitude, depend strongly on these effects. In the cluster models, the interatomic potential within the tip and the surface is assumed to be harmonic, and that between the tip and the surface is taken as being of the Lennard-Jones type. It is clearly shown that AFM images reflect not merely the geometrical structure of the surface, but also various microscopic properties of the tip and the surface.

I. INTRODUCTION

Among various sorts of scanning probe microscopes, the atomic-force microscope[1,2] (AFM) is a powerful tool for the determination of surface structures, because it can resolve both conducting and insulating surfaces in an atomic scale. Therefore AFM is expected to become a basic experimental device not only in the field of surface science but also in many other basic and applied fields such as semiconducting devices, catalyses, electrochemistry, and biological science. In fact, a number of experiments have been successfully done so far on a variety of substrate surfaces—layered materials such as graphite,[3–9] boron nitride[6,7] (BN), and molybdenum disulfide (MoS_2),[6,7] ionic crystals such as NaCl (Ref. 10) and LiF,[11] and even biological substrates such as fibrin,[12] bacterium,[13] and DNA fragments.[14] On the other hand, theoretical studies on AFM have been performed for both rigid surfaces[15–17] and deformable surfaces.[18–25] In these studies, theoretical AFM images were obtained on the calculations such as *ab initio* calculations,[15–17] first-principles calculations,[18–20] molecular relaxation calculations,[21–24] and molecular-dynamics (MD) simulations.[25] An analytical method to express a periodic force field as a Fourier series was also performed.[17,25] Further, the effect of the tip structure was investigated by using several kinds of multiple-atom tips (including the double-atom tip)[21,23–25] and graphite flakes.[22] Many other effects on the AFM images such as load, tip apex structure, bond length of the tip, and tip orientation have been discussed. In particular, Tang, Joachim, and Devillers[24] systematically investigated the effect of the load and tip orientation. However, there still exist some points that have not been made clear yet—detailed features of the force distributions between the tip and surface, effect of the tip apex tilting, and influence of changing the bond length. Therefore, we performed overall studies about these points in the present paper.

As the first step to deal with the AFM mechanism in a systematic way, we performed a theoretical simulation of AFM images in a contact mode. In this work, it is made clear how the AFM images and the force distributions systematically change based on the load variation. Further, the effects of the tip apex structure, the bond length, and the tip orientation are investigated by calculating the AFM images, including the tip and surface deformations. Then the complicated interrelation among them is clearly shown.

In the simulation, a cluster model of a graphite substrate surface with a single-atom tip and two kinds of diamond [111] tips is used. The reason a diamond tip is employed is that a diamond tip is inert and it is used in many AFM experiments. The graphite is one of standard samples to evaluate the performance of AFM. Both the tip and the surface are elastically described by the interatomic harmonic potential. The interaction between the tip and the surface is described by the 6-12 Lennard-Jones pair potential. These potentials are presented with the values of the parameters in Sec. II. Then the total potential energy is minimized by the conjugate gradient (CG) method and the optimized structure of the tip and the surface is obtained. This method is known as a molecular relaxation technique, and it is briefly explained in Sec. III.

In this paper, our main interest is to reveal systematically several microscopic effects on the AFM images as mentioned above: (1) the nonlinear effect of the load with force distributions over the tip and surface atoms, (2) the influence of the tip apex structure and the tip orientation, and (3) the effect of the bond length of the tip as the special case of 2. In Sec. IV, results of calculations about all of these effects are shown. First, the size of the surface cluster is described by comparing the deformations for the different size of surfaces. Then, in the case of a single-atom tip and two kinds of multiple-atom tips, force distributions are directly investigated in order to see the detailed feature causing the total load between the tip and the surface near the contact region. The effective tip

0163-1829/95/52(11)/8471(12)/$06.00

apex structure is varied by the tilt of the tip, which clearly shows the significant dependence of the symmetry of the AFM image on that of the tip apex. This effect is also examined by comparing the results for two kinds of multiple-atom tips. Furthermore, the influence of the bond length is studied by superposing the single-atom images. Lastly, the tip orientation is varied by rotating the tip. This has significant influence on the corrugation amplitude as well as the pattern of the image.

II. MODEL

In this paper, our interest concentrates only on the case of the contact mode with a repulsive force of AFM. Therefore, only the microscopic contact region between the tip and the surface is treated, and the attractive forces coming from the far wider region of the surface and the tip including the cantilever are neglected. Such forces might overcome the repulsive force from the atomistic contact region, but their spatial dependence would be much smoother than the repulsive force. Although the simulation of the AFM images including these forces and the macroscopic cantilever system must be performed, especially for the case of the noncontact mode, this subject will be treated later in our following works.

The cluster model is composed of the tip and the substrate surface. The total energy of the system V consists of the potential energy of the tip V_T, that of the substrate surface V_S, and the tip-surface interaction V_{TS} as follows:

$$V(\{\mathbf{r}_{\rm tip}\},\{\mathbf{r}_{\rm sub}\})=V_T(\{\mathbf{r}_{\rm tip}\})+V_S(\{\mathbf{r}_{\rm sub}\})+V_{TS}(\{\mathbf{r}_{\rm tip}\},\{\mathbf{r}_{\rm sub}\}) , \quad (1)$$

where $\{\mathbf{r}_{\rm tip}\}$ and $\{\mathbf{r}_{\rm sub}\}$ are the positions of the tip atoms and the substrate surface atoms, respectively.

First, V_T is assumed to be a simple harmonic potential for the diamond.[26] It is expressed as the sum of two different types of harmonic terms as follows:

$$V_T(\{\mathbf{r}_{\rm tip}\})=\frac{1}{2}\sum\lambda_r(r_{ij}-r_0)^2+\frac{1}{2}\sum\lambda_\theta r_0^2(\theta_{ijk}-\theta_0)^2 . \quad (2)$$

Here the first term means the bond-stretching energy due to the change of each nearest-neighbor bond length r_{ij} from the equilibrium one r_0. The second term represents the bond-bending energy corresponding to the change of each bond angle θ_{ijk} from the equilibrium one θ_0. The parameters of V_T are $r_0=1.5445$ Å, $\lambda_r=29.512$ eV/Å^2, $\theta_0=\cos^{-1}(-1/3)$rad, and $\lambda_\theta=3.5213$ eV/Å^2. The microscopic parameters λ_r and λ_θ were determined by Harrison[26] from the elastic constants c_{11}, c_{44}, and c_{12} based on the classical theory of elasticity. Mcskimin and Bond[27] observed these macroscopic constants by means of ultrasonic waves.

Similarly, V_S is also assumed to be a harmonic potential for the graphite,[28] which consists of four different types of harmonic terms as follows:

$$V_s(\{\mathbf{r}_{\rm sub}\})=\frac{1}{2}\sum\mu_r(r_{ij}-r_0)^2+\frac{1}{2}\sum\mu_\theta r_0^2(\theta_{ijk}-\theta_0)^2+\frac{1}{2}\sum\mu_d(d_{ij}-d_0)^2+\frac{1}{2}\sum\mu_p\left[\delta z_i-\frac{\delta z_j+\delta z_k+\delta z_l}{3}\right]^2 . \quad (3)$$

This potential was used by Yoshimori and Kitano[28] in order to study the lattice vibration and specific heat of graphite. Similar to V_T, the first and second terms correspond to the bond-stretching and the bond-bending energy, respectively. θ_{ijk} denotes the angle between the bond i-j and the bond j-k within the same honeycomb net plane. The third term is the interlayer bond-stretching energy for the change of the interlayer distance d_{ij} from the equilibrium distance d_0. The fourth term is the bending energy of the local planar structure due to the normal displacement of the ith atom from the plane made of the three neighboring atoms j, k, and l; δz_i denotes the normal displacement of the ith atom from the initial position. The parameters of V_S are assumed to be $r_0=1.4210$ Å, $\mu_r=41.881$ eV/Å^2, $\theta_0=2\pi/3$ rad, $\mu_\theta=2.9959$ eV/Å^2, $\mu_d=0.347\,65$ eV/Å^2, $d_0=3.3539$ Å, and $\mu_p=18.225$ eV/Å^2, respectively. The values of μ_r and μ_θ were estimated by Komatsu and Nagamiya[29] from the observed force constants of planar vibrations of benzene molecule. Those of μ_d and μ_p were determined by Yoshimori and Kitano.[28] Komatsu[30] estimated the quantities containing μ_d and μ_p, from the observed compressibility and the specific heat, respectively.

The sum of the 6-12 Lennard-Jones potential is chosen for V_{TS}, i.e.,

$$V_{TS}(\{\mathbf{r}_{\rm tip}\},\{\mathbf{r}_{\rm sub}\})=\sum_{i,j}v_{TS}(|\mathbf{r}_{{\rm tip},i}-\mathbf{r}_{{\rm sub},j}|)=\sum_{i,j}4\epsilon\left[\left[\frac{\sigma}{r_{ij}}\right]^{12}-\left[\frac{\sigma}{r_{ij}}\right]^{6}\right] . \quad (4)$$

Here, we assume that every tip atom interacts with all the surface atoms only through a pair potential and that this potential is the same for all the pairs of the tip and the substrate surface atoms. Although the parameters ϵ and σ are not necessarily unique, those used by Gould, Burke, and Hansma[23]—$\epsilon=0.873\,81\times10^{-2}$ eV and $\sigma=2.4945$ Å—are employed. The merit of this potential is that the corrugation amplitude is well reproduced. This potential is used with a cutoff at $r_c=2.3\sigma$.

Thus, the total potential V chosen in the simulation does not include the torsion energy and intrabulk van der Waals interaction except the nearest interlayer interaction of the graphite. In this point, V is different from those of molecular-mechanics models.[31]

III. METHOD OF CALCULATION

In this section, the method of calculation is briefly explained. First, the tip is placed above the substrate surface. Then the total energy V is minimized by using the Polak-Ribiere–type conjugate gradient method.[31] The CG method is one of the most efficient methods of multidimensional minimizations. This structual optimization is called a molecular relaxation technique. Then the total force $\mathbf{F}(z)$ acting on the tip is obtained for the respective values of z. Here z is the coordinate parallel to the [111] axis of the diamond, that is to say, perpendicular to the graphite [0001] plane, as shown in Fig. 2. The details of the diamond-graphite cluster are mentioned in Sec. IV. In our calculation, only the perpendicular deflection of the cantilever is allowed, and we focus on the z component of $\mathbf{F}(z), F_z(z)$. Because of the flatness and the symmetry of the graphite surface, the calculated lateral components $F_x(z)$ and $F_y(z)$ are actually a few orders of magnitude lower than $F_z(z)$ and can be neglected. Here we set the convergence criterion as the maximum of absolute values of all the forces acting on the movable atoms that is lower than 10^{-5} nN, i.e.,

$$\max_{1\le i\le N}(|\mathbf{F}_i|)<10^{-5}\ \text{nN}\ , \tag{5}$$

where N is the total number of movable atoms both of the tip and the substrate surface, and $\mathbf{F}_i$ is a force acting on the ith atom.

We performed calculations as mentioned above for several z values for a fixed (x,y). Further, according to the method adopted by Tang, Joachim, and Devillers,[24] z-F_z relation (force curve) is obtained by a polynomial fit from F_z values corresponding to these z values. The sixth order polynomial is used and the residue of this fitting is less than the order of 10^{-5} nN. Then the equation

$$F_z(z)=F_{\text{sc}} \tag{6}$$

is solved and the tip height z for the scanning force F_{sc} is calculated. If this procedure is repeated for (x,y) values in the region of the tip scanning, the AFM image with a constant scanning force of F_{sc} can be made. On the other hand, when z is fixed, the constant height image is obtained.

Lastly, since the potential V derives from the harmonic approximation, our calculation is valid only when the atomic displacements are relatively small. Therefore, about 5 nN is the maximum repulsive force we can treat in our calculation. We are basically interested in the deformation under the comparatively weak loading conditions. In a much stronger loading regime, it can be thought that the qualitative nature of the present results based on the harmonic potential V is not very different from that based on the potential suitable for the stronger force regime. We want to study only the general features of the AFM images.

IV. RESULTS AND CALCULATIONS

A. Three kinds of tip and the size of the surface

Considering the symmetry, the cluster model of the graphite surface is made by adding hexagons around the center hexagon. If the surface deformation near the tip-surface contact region is noticed, the small surface cluster with 96 cluster atoms per layer is enough for the AFM simulations. In order to confirm this, the deformation of the monolayer surface is calculated. First, a single-atom tip is placed right above the atom of two kinds of clusters—the small cluster composed of 96 atoms and the large cluster composed of 600 atoms. All of the edge atoms of both the clusters are fixed. Then, as shown in Fig. 1(a), the tip is moved closer to the surface. The surface deformations near the tip in the case of $F_z=5$ nN are presented in Figs. 1(b-1) and 1(b-2). It can be said that the deformed large cluster with 600 atoms is approximately obtained simply by translating the deformed small cluster with 96 atoms parallel to the z axis as seen in Fig. 1(b-2). Thus, surface deformations near the tip

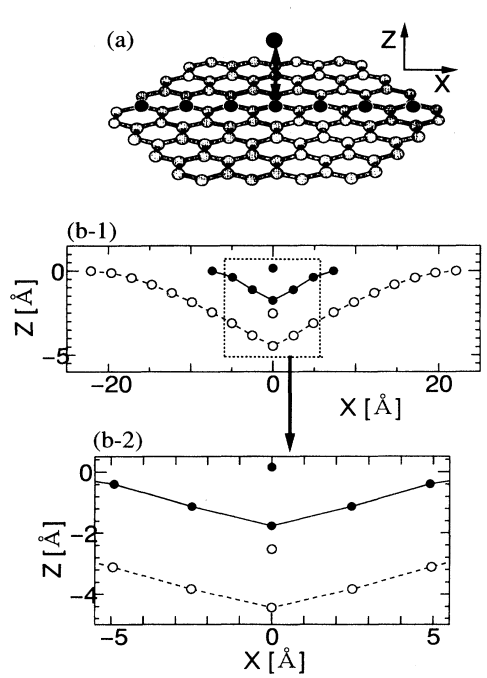

FIG. 1. (a) The cluster model of the single-atom tip and of the monolayer surface made up of 96 atoms. Z is the direction parallel to the [0001] axis, and denotes the distance between the tip atom and the surface atom right below it before the surface relaxation. (b-1) The deformations of the monolayer surface with 96 atoms and with 600 atoms. The x and z coordinates of the tip and the surface are illustrated. Black circles and the solid line correspond to the case of the surface with 96 atoms, and white circles and the dashed line to the case of the surface with 600 atoms. (b-2) Surface deformations near the tip corresponding to the dashed line box in (b-1).

can be described rather accurately even by the comparatively small cluster made up of 96 atoms.

Therefore, as a cluster of the substrate surface, the graphite made up of 288 atoms with three layers, each of which consists of 96 atoms, is used. As a boundary condition, all of the 96 atoms of the third layer, and 42 atoms on the edges of the first and the second layers, are fixed. Following the standard nomenclature of bulk graphite, the atomic site of the first layer just under which there exists an atom or not is designated as the A or the B site, respectively. And the center of the hexagon is called the H site.

Then, the single-atom tip and two kinds of multiple-atom diamond [111] tips are used. The example of the AFM cluster system used in our calculation, with a diamond tip made up of 54 atoms, is presented in Fig. 2. The diamond [111] tip made up of 50 atoms is shown in Fig. 3. The effect of the reconstruction of the tip surface is neglected.

B. Single-atom tip

The model of the single-atom tip, which represents the virtual sharpest tip, is first calculated for the comparison with the results of more realistic tip models. Figures 4(a-1) and 4(b-1) show the images with a constant scanning force of 0.5 and 5.0 nN, respectively. Both images show honeycomb lattice patterns. The corrugation amplitude Δz_{AH} (the difference in the tip height between the A and the H sites) is about 0.2 Å. This calculated corrugation 0.2 Å is of the same order as the experimental one 0.15 Å obtained by Albrecht and Quate[7] in air. In these images, the effect of the mechanical interlayer interaction is so weak that there seems little difference between the A and B sites. Then, force distributions are calculated in order to see why the image of the total force that the tip detects is different in these two cases. In a weak repulsive force of $F_z = 0.5$ nN, a single-atom tip right above the A site approximately detects a force from only the A site as shown in Fig. 4(a-2). In this case, the single-atom contact occurs. This means that the honeycomb image of Fig. 4(a-1) directly reflects the geometrical surface structure. In a strong repulsive force of $F_z = 5.0$ nN, Fig. 4(b-1) also presents a honeycomb pattern similar to Fig. 4(a-1). But in this case, the image of the A site is made up of forces from four surface atoms—one A site and three B sites which are nearest neighbors of the A site as shown in Fig. 4(b-2). About 79% of F_z derives from the A site, and the other from three B sites as shown in Fig. 5. Thus, although the single-atom contact begins to break, atomic resolution is still achieved.

In Figs. 4(a-1) and 4(a-2), the A sites are as bright as the B sites. Furthermore, the hexagonal rings are also clearly seen. However, such perfect honeycomb patterns are not observed in the experiments. Even nearly honey-

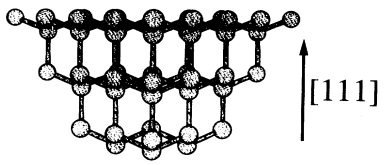

FIG. 3. Multiple-atom tip made up of 50 atoms.

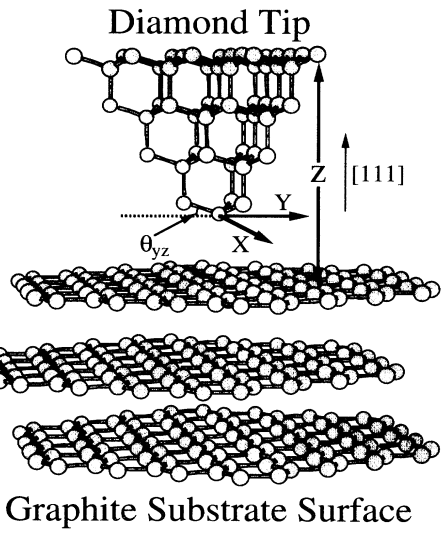

FIG. 2. The cluster model of the diamond [111] tip made up of 54 atoms and the graphite surface. Z denotes the vertical distance between the fixed basal plane of the tip and the first layer of the surface before relaxation. θ_{xy} is a tilt angle of the tip.

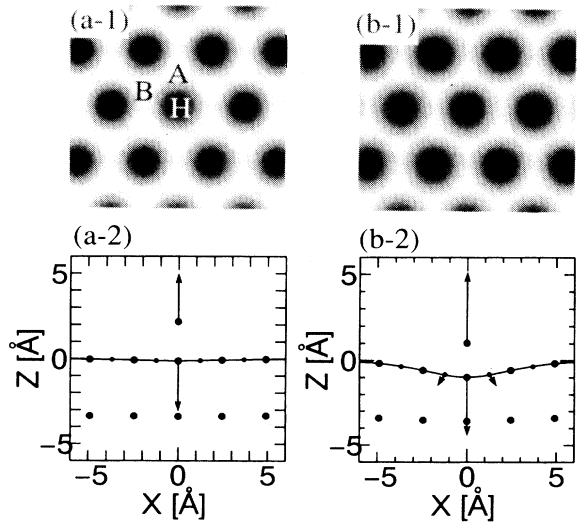

FIG. 4. Constant-force images and force distributions for a single-atom tip. The scanning force F_z is a weak repulsive force of 0.5 nN for (a-1) and (a-2), and a strong repulsive force of 5.0 nN for (b-1) and (b-2). In (a-1) and (b-1), the lateral dimensions are 8 Å×8 Å. In (a-2) and (b-2), the single-atom tip is placed right above the A site. Only the x and z components of the atomic sites and the forces are shown. The larger black circles represent surface A sites or tip atoms, and the smaller black circles represent surface B sites.

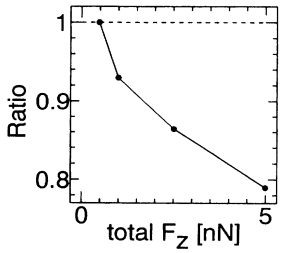

FIG. 5. The ratio of the vertical force originating from the A site to total F_z, when a single-atom tip is placed right above the A site. In the case of $F_z=5.0$ nN, 79% of F_z originate from the A site, and the other from three B sites (the nearest neighbors of the A site).

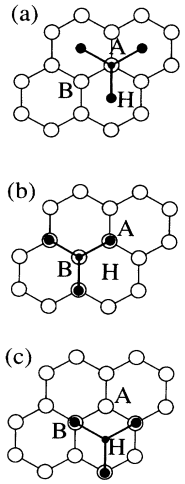

FIG. 6. Multiple-atom tip made up of 54 atoms positioned on the (a) A, (b) B, and (c) H sites. The large and the small black circles correspond to the first- and the second-layer tip atoms, respectively. The white circles correspond to the graphite atoms.

comb images are observed only in some experiments,[3,7] and a variety of deformed images, that is to say, anomalous images, has been obtained for graphite surfaces. Therefore, the single-atom tip is too ideal to model the AFM tip. Several authors have well reproduced anomalous images by using a graphite flake[22] or multiple-atom tips.[21,23–25] In the following section, two kinds of multiple-atom tips are used to study more realistic effects on AFM images.

C. Multiple-atom tip made up of 54 atoms

One of two multiple-atom tips is made up of 54 atoms with the axis parallel to the diamond [111] direction. This tip consists of eight layers, and has one apex atom and three atoms in the second layer as shown in Fig. 2. The calculated results with this tip, such as force curve and image patterns, are qualitatively similar to those with a 13-tip apex used by Tang, Joachim, and Devillers.[24] In the present paper, we report the results of simulation using the 54-tip apex. The tip orientation is fixed as shown in Figs. 6(a)–6(c). In this orientation, force F_z versus distance z curves are presented in Fig. 7. We note that z is defined as shown in Fig. 2. At a certain load F_z, the H site is lower than the A and B sites. The B site is a little higher than the A site. The reason for the difference of height between the three sites is explained below, with the interpretations of AFM images. The tip detects forces mainly by one apex atom and by three atoms of the second layer [Figs. 8(a-2) and 8(b-2)]. In a weak repulsive force of $F_z=0.5$ nN, one apex atom detects the dominant repulsive forces, and three atoms of the second layer feel rather small attractive forces [Fig. 8(a-2)]. Therefore, the forces between the tip and the surface approximately concentrate only on one atom of the tip and the surface, and the single-atom contact occurs, similar to the case of the single-atom tip. However, as F_z increases, repulsive forces distribute over many atoms. In a strong repulsive force of $F_z=5.0$ nN, the forces felt by three atoms of the second layer also become repulsive and larger, and multiple-atom contact occurs [Fig. 8(b-2)]. However, the image reflects the periodicity of the graphite lattice and has an atomic resolution [Fig. 8(b-1)]. With further increase of the net force, the tip detects a mixing of repulsive forces distributed over a wider region.

Although the interpretation of the calculated images is generally difficult, the brightness of the site in the particular example mentioned above is explained by the location of the tip atoms. For the case of $F_z=0.5$ nN, the simulated image shows basically a honeycomb lattice pattern, in which the B site is a little brighter than the A site if we look at the image closely [Fig. 8(a-1)]. This image is similar to an experimental image.[7] When the tip is placed above the A site, three atoms of the second layer of the tip are located above neither the A site nor the B site as shown in Fig. 6(a). In this case, the attractive forces between the surface and the second layer of the tip become larger when the tip is placed above the A site than those obtained when the tip is situated above the B site [Fig. 6(b)]. However, the repulsive force between the surface and the tip apex atom above the A site is almost equivalent to that for the tip above the B site. Therefore,

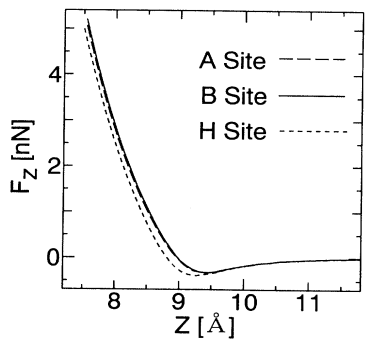

FIG. 7. Force F_z vs distance z curves on A, B, and H sites for a multiple-atom tip made up of 54 atoms.

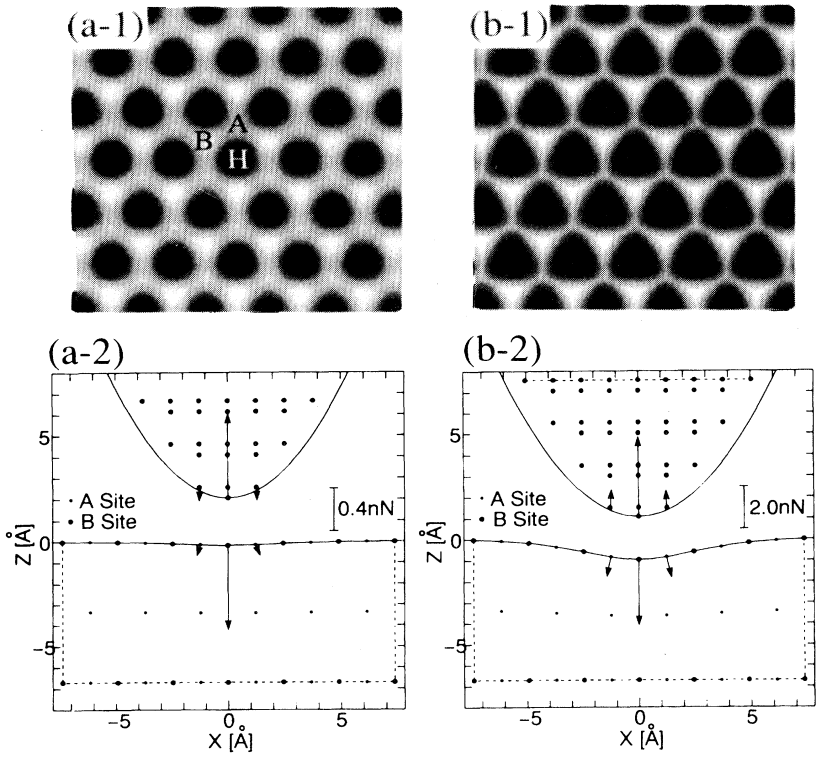

FIG. 8. The same as Fig. 4 for a multiple-atom tip made up of 54 atoms. In (a-1) and (b-1), the lateral dimensions are 13 Å×13 Å. In (a-2) and (b-2), the tip is placed right above the B site. The larger black circles represent surface B sites or tip atoms, and the smaller black circles represent surface A sites. The solid line denotes the section of the paraboloid that includes four tip apex atoms. The broken lines denote the boundary of the cluster models.

the net repulsive forces above the B sites are larger than those above the A sites. With the increase of F_z, the trend of a triangular lattice pattern becomes enhanced. In the case of $F_z=5.0$ nN, we notice that the bright spots show almost triangular shapes, and that the wire net pattern that combines the A and the B sites is also presented [Fig. 8(b-1)]. This image corresponds well to the experimental image.[3] When the tip is placed above the B site, each of the three tip atoms of the second layer can easily interact with the A site as shown in Fig. 6(b). In this location, the repulsive forces between the surface and the second layer of the tip become the largest. Furthermore, the effect of the interlayer interaction becomes more enhanced in the case of Fig. 8(b-1) than the case in Fig. 8(a-1). Thus, the net repulsive forces above the B sites are larger than those above the A sites. In this strong repulsive force mode, the physical quantity represented by the AFM image is the sum of the forces distributed over many atoms that are self-consistently determined, together with the microscopic atomic deformations of both the tip and the surface. Therefore its correspondence with the surface corrugation is rather complicated and a simple explanation is rather difficult.

The corrugation amplitude Δz_{BH} (the difference in the tip height between the B and the H sites) is about 0.14 Å for Fig. 8(a-1), and 0.08 Å for Fig. 8(b-1). The reason the corrugation for the strong repulsive force is smaller than that for the weak repulsive force is probably that the edge effect is negligible for the multiple-atom tip even at $F_z=5.0$ nN.

The effects of the tip apex structure on the image are also investigated by the tilt of the tip. The tilt of the tip causes the change of the tip apex geometry, which influences the net forces between the tip and the surface. The tip is tilted around the axis parallel to the x axis passing the tip apex atom. The tilt angle is denoted as θ_{yz} presented in Fig. 2, and it is varied from 19.5° to 0°. At the respective θ_{yz}, the tip is scanned with a constant force of 0.1 nN. At $\theta_{yz}=19.5°$, an effective tip is composed of one apex atom and three atoms in the second layer, and it has threefold symmetry. On the other hand, when $\theta_{yz}=0°$, the tip consists of two apex atoms and two second layer atoms, and it has twofold symmetry. Corresponding to this change of the tip apex symmetry, the threefold symmetry of AFM images also turns into twofold symmetry as shown in Figs. 9(a)–9(d) in the order of θ_{yz}=(a) 19.5°, (b) 10°, (c) 5°, and (d) 0°. With the decrease of θ_{yz}, the A sites become darker and the stripes become brighter. Figure 9(d) is obtained because the forces are distributed dominantly on two apex atoms of the tip as shown in Fig. 10. This image corresponds well to the experimental images.[6,7] The theoretical simulation with simpler diatom tips also reconstructed such images.[17,23] When the tip is placed right above the B site, both apex atoms are located nearly above the surface sites. But above the A or the H site, only one of the two apex atoms is located above the A or the B site, respectively. Therefore, only the regions near the B sites become bright. But in fact, if we look at Fig. 9(d) closely, we notice that the bright spots in Fig. 9(d) do not perfectly match the real atomic sites. Because the bond length of the diamond is about 0.1 Å larger than that of the graphite, the bright

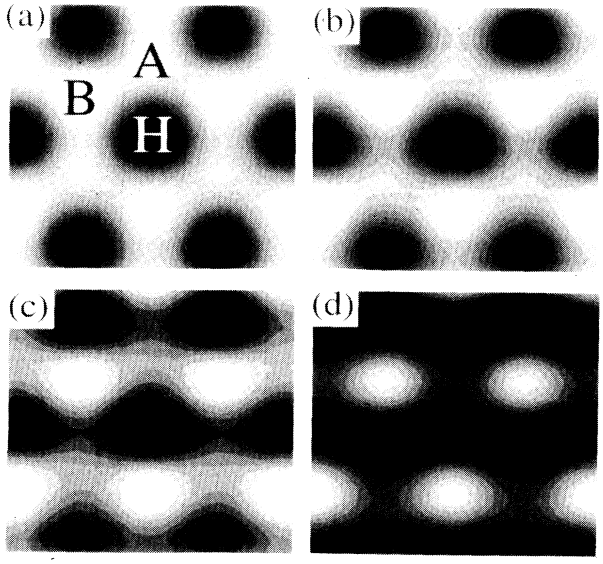

FIG. 9. Constant-force image for a multiple-atom tip made up of 54 atoms with the scanning force of 0.1 nN. The tilt angle θ_{yz} is (a) 19.5°, (b) 10°, (c) 5°, and (d) 0°. The lateral dimensions are 5 Å×5 Å.

spots of the B sites of Fig. 9(d) are located at about 0.1 Å higher than those of Fig. 9(a) in the vertical direction.

D. Multiple-atom tip made up of 50 atoms

The other model of a multiple-atom tip is made up of 50 atoms parallel to the [111] axis. This tip consists of six layers, and has three apex atoms and six atoms in the second layer as presented in Fig. 3. Therefore it is a rather dull tip. The tip orientation is fixed as shown in Figs. 11(a)–11(c). This tip detects forces mainly by three apex atoms and by six atoms of the second layer [Fig. 12(b)]. The image of the graphite surface with a scanning force of 0.5 nN shows a honeycomb lattice [Fig. 12(a)]. In this image, both the B and the H sites are brighter than the A sites. Similar to the case of the tip made up of 54 atoms, the brightness of the site is explained as follows: When the tip is placed above the H site, three first-layer atoms and six second-layer atoms easily interact with the B and the A sites, respectively [Fig. 11(c)]. Above the B site, only three apex atoms significantly interact with the A sites [Fig. 11(b)]. However, when the tip is placed above the A site, only six atoms of the second layer are located above the B sites [Fig. 11(a)]. Therefore, the repulsive tip-surface interaction above the B and the H sites becomes larger than that for the case with the tip placed above the A site. The corrugation amplitude Δz_{HA} is 0.14 Å, and the H site is as bright as the B site. Thus, although multiple-atom contact occurs, even the rather dull tip can observe a honeycomb lattice similar to that obtained by a single-atom tip with a single-atom contact. Unlike the image of the single-atom tip, the bright spots do not match the real atomic sites any longer. Though the A sites are atomic sites, the image of the A sites is dark. This dull tip observes the forces distributing over a wider region than the multiple-atom tip made up of 54 atoms as shown in Fig. 12(b). However, in the orientation mentioned above, the projection of the tip apex to the surface is nearly commensurate with the graphite lattice, and eventually the honeycomb image is obtained. Therefore, this image [Fig. 12(b)] reflects the periodicity of the graphite lattice. We should be careful that the periodic AFM images can be always obtained with an unusual tip as used here, if the surface has an ideal two-dimensional translational symmetry. The tip apex structure is an important factor in determining the contact condition and the region of force distributions.

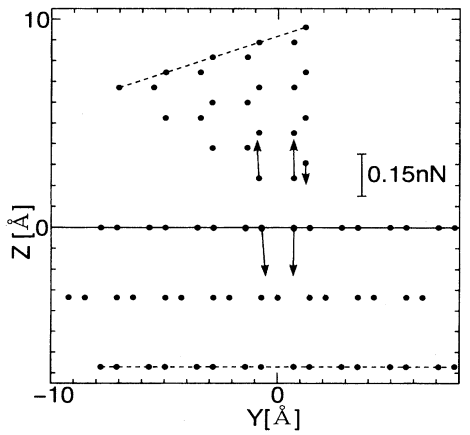

FIG. 10. Force distributions for a weak repulsive force of $F_z = 0.1$ nN when the tilt angle θ_{yz} is 0°. The y and z coordinates of the atomic sites and of the forces are presented.

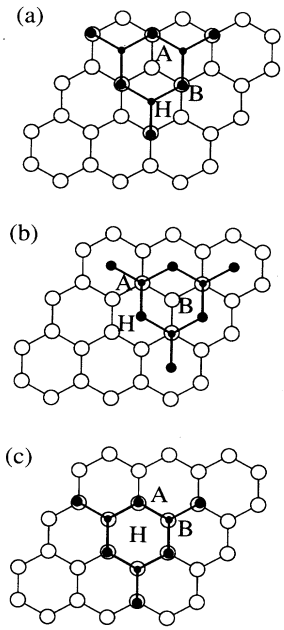

FIG. 11. The same as Fig. 6 for the multiple-atom tip made up of 50 atoms.

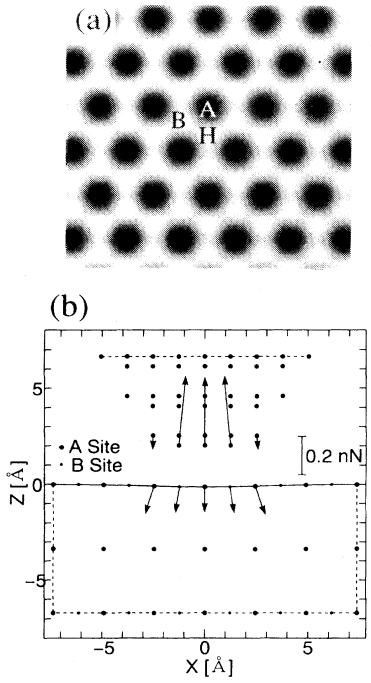

FIG. 12. (a) Constant-force image and (b) force distributions for a multiple-atom tip made up of 50 atoms. F_z is a weak repulsive force of 0.5 nN. In (a), the lateral dimensions are 13 Å×13 Å. In (b), the multiple-atom tip is placed right above the A site. Only the x and z components of the atomic sites and the forces are shown. The larger black circles represent surface A sites or tip atoms, and the smaller black circles represent surface B sites. The broken lines denote the boundary of the cluster models.

E. The effect of the bond length of the tip

In this section, the effect of the bond length of the tip on the AFM image is investigated as the special case of a tip apex structure. First, it is shown that the AFM image for a double-atom tip in a weak repulsive force mode is approximately reproduced by superposing two single-atom tip images. Then the results of the superposition of two images are presented. Figure 13(a) shows a force image with a single-atom tip scanned at a constant height of $z=2.3$ Å. This is a constant-height mode in a weak repulsive force and the maximum value of detected forces is about 0.26 nN. Therefore the deformation of the tip and the surface is small. When this image, in other words z components of the forces at $\mathbf{r}=(x,y)$, is denoted as $F_1(\mathbf{r})$, $F_1(\mathbf{r}-\mathbf{r}_T)$ is obtained by moving Fig. 13(a) parallel to $\mathbf{r}_T$ in the (x,y) plane. The superposition of two images $F_2(\mathbf{r})$ is represented as

$$F_2(\mathbf{r})=F_1(\mathbf{r})+F_1(\mathbf{r}-\mathbf{r}_T)\ .$$

First, $F_2(\mathbf{r})$ is calculated in the case of $\mathbf{r}_T=(0,5d_0)$ as shown in Fig. 13(f). Here $d_0=a_0/4$, and a_0, the bond length of the graphite, is 1.421 Å. Then, $5d_0$ is about 1.776 Å. This constant-height image is very similar to the constant-force image of Fig. 9(d). Figure 9(d) is obtained by the tilt of the tip and the effective tip detecting forces approximately equals a double-atom tip with a bond length of diamond, 1.545 Å. Therefore, Fig. 13(f) made by superposition can be assumed to be obtained by scanning of a double-atom tip with a bond length of $5d_0=1.776$ Å. However, it should be noticed that this superposition goes well because the deformation of the surface and the tip is small in a weak repulsive force. If the load F_z increases and the deformation becomes large, this simple superposition is invalid. Thus, the weak repulsive force image of the constant-height mode for a double-atom tip whose bond length is $|\mathbf{r}_T|$ and whose orientation for the surface is $\mathbf{r}_T$ is approximately reproduced by superposing two single-atom tip images, $F_1(\mathbf{r})$

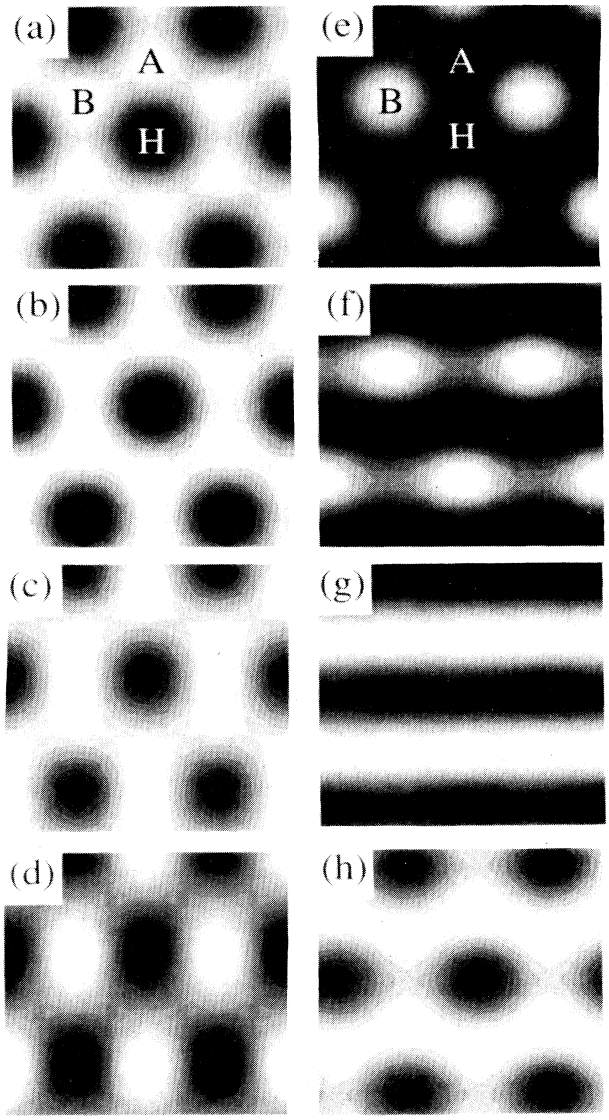

FIG. 13. (a) Constant-height image with a scanning of a single-atom tip at $z=2.3$ Å. Sum of two (a)'s in the case of $\mathbf{r}_T=$(b) $(0,d_0)$, (c) $(0,2d_0)$, (d) $(0,3d_0)$, (e) $(0,4d_0)$, (f) $(0,5d_0)$, (g) $(0,6d_0)$, and (h) $(\sqrt{3}d_0,0)$. Here $a_0=1.421$ Å and $d_0=a_0/4$. The lateral dimensions are 7 Å×7 Å.

and $F_1(\mathbf{r}-\mathbf{r}_T)$. Of course, both atoms of the double-atom tip are located in the same plane parallel to the (x,y) plane.

Then, in order to see the effect of the bond length of the tip, $\mathbf{r}_T$ is varied. $F_2(\mathbf{r})$ is calculated for $\mathbf{r}_T=(0,d_0)$, $(0,2d_0)$, $(0,3d_0)$, $(0,4d_0)$, $(0,6d_0)$, and $(\sqrt{3}d_0,0)$. Each case corresponds to Figs. 13(b), 13(c), 13(d), 13(e), 13(g), and 13(h), respectively. It is clearly shown that the bright spots in these images, except for Fig. 13(e), do not match the real atomic sites. When $|\mathbf{r}_T|$ is small $[\mathbf{r}_T=(0,d_0)]$, the image is still a honeycomb pattern a little extended in the vertical direction [Fig. 13(b)]. But $|\mathbf{r}_T|$ is increased still more $[\mathbf{r}_T=(0,2d_0)$ and $(0,3d_0)]$ and the sum images become triangular arrays of rectangles as shown in Figs. 13(c) and 13(d), respectively. Figure 13(d) is analogous to the previously calculated images reported in Refs. 17 and 22. In the case of MoS_2 and BN, similar images have also been observed.[6,7] When $|\mathbf{r}_T|$ becomes equal to the lattice constant of the graphite $[\mathbf{r}_T=(0,4d_0)]$, both the B sites of $F_1(\mathbf{r})$ and the A sites of $F_1(\mathbf{r}-\mathbf{r}_T)$ enhance each other. Therefore the image becomes a triangular array of spheres and the bright spots match the real surface B sites as shown in Fig. 13(e), corresponding to the experimental images.[6,7] As $|\mathbf{r}_T|$ is increased still more $[\mathbf{r}_T=(0,5d_0)]$, the wavelike stripe parallel to the x direction, which links the bright spots, appears. In this case, the bright spots become ellipses [Fig. 13(e)]. This image is very similar to the constant force image of Fig. 9(d) as mentioned above. In the case of $\mathbf{r}_T=(0,6d_0)$, the image becomes a perfect straight stripe [Fig. 13(g)]. This image appears because the H site of $F_1(\mathbf{r})$ is located on the middle point between two H sites of $F_1(\mathbf{r}-\mathbf{r}_T)$. This image is also reported by another theoretical calculation.[17] Furthermore, similar images were observed for BN.[6] Then $F_1(\mathbf{r})$ is moved parallel to the x direction. In the case of $\mathbf{r}_T=(\sqrt{3}d_0,0)$, the image is a honeycomb one where the wavelike stripe can clearly be seen [Fig. 13(h)]. For $\mathbf{r}_T=(2\sqrt{3}d_0,0)$, the image becomes the same as in Fig. 13(g). This wavelike image is a modified honeycomb pattern often observed in experiments.[3,7,9]

Thus a variety of images mentioned above is caused by the enhancement of the surface sites of two force images whose phases are different from each other. Therefore, it can be concluded that the AFM image is very sensitive to the bond length of the tip. The effective structure of the tip apex mainly detecting the forces is especially important. In this section, only the case in which two atoms are in the same plane parallel to the x-y plane is treated. By changing the weight of the superposition of the two images, a more general case, where two atoms are in different planes, can be discussed. But we will make this argument in a future work.

F. The effect of the tip orientation

Finally, the effects of the tip rotation around its axis on the image are investigated for two kinds of multiple-atom tips. First, results of the case for the multiple-atom tip made up of 54 atoms are mentioned. When the tip is rotated clockwise around the [111] axis parallel to the z axis with a scanning force of 0.5 nN (Fig. 14), the image varies as shown in Figs. 15(a)–15(d). The definition of θ_{xy} is illustrated in Fig. 14. At $\theta_{xy}=0°$, the B sites is brighter than the A site [Fig. 15(a)], and the corrugation amplitude is about 0.13 Å. As θ_{xy} increases, the difference of the brightness between the A and the B site decreases [Fig. 15(b)]. At $\theta_{xy}\simeq 30°$, the A site is approximately as bright as the B site and the image becomes a nearly perfect honeycomb lattice pattern [Fig. 15(c)]. In our calculation, the precise angle where the A site is exactly as bright as the B site is about 27°. When θ_{xy} increases still more, the A site becomes brighter than the B site and the corrugation amplitude becomes larger and takes the maximum value, 0.15 Å at $\theta_{xy}\simeq 35°$. These results show the mechanical inequality between the A and the B sites based on the interlayer interaction. At $\theta_{xy}=60°$, the brightness of the A and B sites is perfectly reversed compared to the case of $\theta_{xy}=0°$ [Fig. 15(d)], and the corrugation is about 0.14 Å. Thus AFM images reflect the rotation of the tip for 60°, and the rotation causes the reverse of the site brightness between the A and the B sites. This reverse is caused mainly by the interaction between three second-layer atoms of the tip and the surface sites.

Then, the rotation of the multiple-atom tip made up of 50 atoms is performed. This tip has three atoms on the truncated plane of its apex. Therefore, the rotation of this dull tip deals with a more general case than the one treated in the work of Paik, Kim, and Schuller.[25] Paik, Kim, and Schuller performed a MD simulation for a simple triangular tip and obtained images similar to Figs. 16(a)–16(c). Furthermore, they also calculated a tip-surface interaction based on a Fourier series, and obtained a similar relation to the solid line of Fig. 17. The influence of the tip orientation is rather different from that for the tip made up of 54 atoms. The tip is also rotated clockwise around the [111] axis with a scanning force of 0.1 nN. The image varies as shown in Figs. 16(a)–16(c). For this tip, the brightness between the A and the B sites for $\theta_{xy}=60°$ is also perfectly reversed compared to that for $\theta_{xy}=0°$, similar to the case of the tip made up of 54 atoms. At $\theta_{xy}=0°$, the tip is commensurate with the surface and the honeycomb image is obtained as shown in Fig. 16(a). In this case, the corrugation amplitude is about 0.17 Å. However, when θ_{xy} increases, the tip apex structure becomes incommensurate with the surface, and the corrugation amplitude becomes

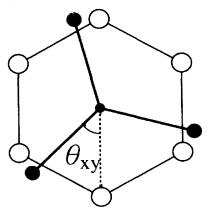

FIG. 14. The rotational angle θ_{xy} of the tip. The smaller black circles denote the tip apex atoms and the larger black circles denote the atoms of the second layer of the tip. The white circles denote surface atoms.

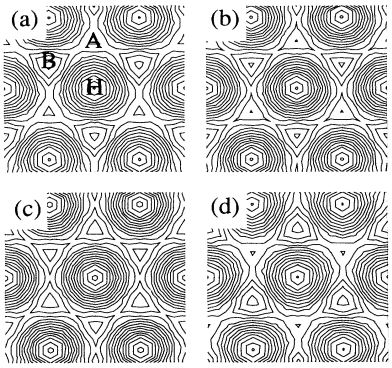

FIG. 15. Constant-force image for a contour plot expression with $N_T=54$ and $F_z=0.5$ nN. The rotational angle θ_{xy} is (a) 0°, (b) 20°, (c) 30°, and (d) 60°. The lateral dimensions are 5 Å×5 Å.

smaller. At $\theta_{xy}=10°$, the corrugation of the image changes a little [Fig. 16(b)]. However, at $\theta_{xy}=20°$, the corrugation rapidly decreases and the image becomes rather dark [Fig. 16(c)]. At $\theta_{xy}\simeq 30°$, the tip apex structure becomes the most incommensurate with the surface and the corrugation takes the minimum—0.01 Å. Therefore, although the image still has threefold symmetry, it can be thought that the image for this orientation cannot be observed in the experiment [Fig. 16(c)]. This restricts the region of rotation angle for observing the AFM images, and the region in which AFM images are impossible to obtain appears at every 60°.

If a small load is applied to a dull tip, the difference between the A and the B sites hardly occurs, unlike in the case of the tip made up of 54 atoms. The corrugation amplitude as a function of the tip orientation (θ_{xy}) is presented in Fig. 17. The difference between the maximum and the minimum corrugation for the tip made up of 54 atoms—0.01 Å—is much smaller than that for the tip made up of 50 atoms. Thus, although the AFM image is sensitive to the tip rotation, the sensitivity to the tip orientation depends strongly on the tip apex structure.

V. SUMMARY AND CONCLUSION

In this paper, we performed a theoretical simulation of AFM images in the repulsive force mode based on cluster models. From this calculation, several fundamental features of the effects on the AFM images are systematically clarified. Generally speaking, AFM images not only represent the surface geometrical structures, but also are influenced by many other microscopic features of the tip and the surface such as the force distributed over atoms in the contact region, deformation, tip apex structure, bond length, and orientation. The cluster system used in our calculation represents only the microscopic contact region of the tip surface, and neglects the macroscopic region of the surface and tip including the cantilever. Nevertheless, the calculated AFM images are consistent with the experimental images. This probably means that AFM of a contact mode in a repulsive force region is strongly dependent on the short-range interatomic forces. However, it should be remarked that, in the actual experiments, the repulsive forces detected by the tip apex are screened by the long-range attractive forces, which are almost constant in the atomic scale. Under certain condi-

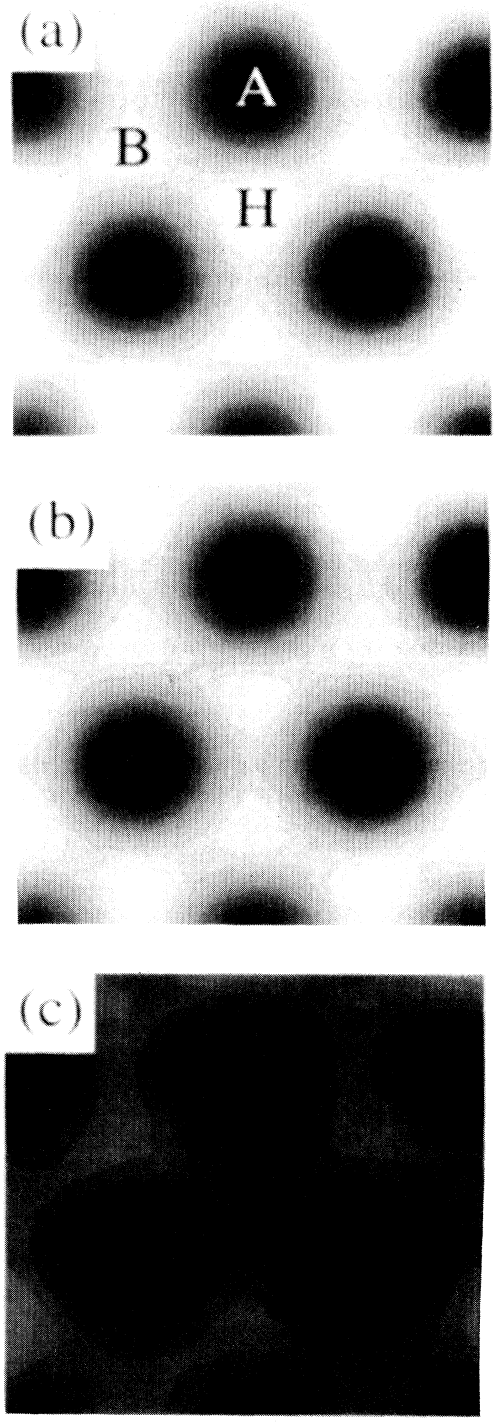

FIG. 16. The same as Fig. 15 for gray-scale expression with $N_T=50$ and $F_z=0.1$ nN. The lateral dimensions are 5 Å×5 Å.

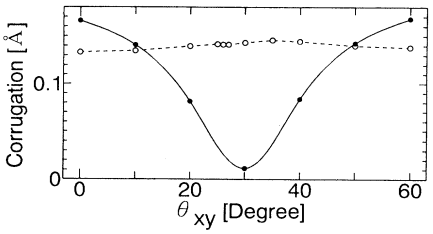

FIG. 17. Corrugation amplitude as a function of the rotational angle θ_{xy} for (a) $N_T=54$ and $F_z=0.5$ nN (white circles), and (b) $N_T=50$ and $F_z=0.1$ nN (black circles). Here N_T is the number of tip atoms and F_z is a scanning force.

tions the latter overcomes the former, then the atomistic AFM image can be obtained even in the attractive-force mode. Therefore the macroscopic effects of the system are necessary to deal with the AFM mechanism of a noncontact mode.

Then, it is made clear how the transition from a single-atom contact to a multiple-atom contact occurs as the load increases. The tip apex structure is also investigated. Even when multiple-atom contact occurs, the honeycomb image, which is very similar to that observed by a single-atom tip, is obtained in a specific orientation, because the tip apex structure is commensurate with the surface. Therefore, the commensurateness between the tip and the surface is very important for the atomic resolution of the images. However, the bright spots in the image do not necessarily correspond to real atomic sites. In this case, the interpretation of the image becomes complicated, and the quantities represented by AFM images are not necessarily simple. Furthermore, the possibility to evaluate the tip apex structure is revealed by tilting or rotating the tip. For example, in the case of a dull tip that has three atoms on the tip apex, the corrugation amplitude rapidly decreases at a specific range of the orientation. In particular, the study of the corrugation by rotating the tip can be easily performed in experiments. We also note a standard process to study the surface structure based on theoretical images as follows: First, the tip is scanned on a well-defined surface such as graphite and, comparing experimental images with theoretical ones obtained in calculations such as ours, the tip apex structure can be identified. Then the tip is scanned on a substrate surface one should actually observe, and obtained images can be analyzed based on the tip apex structure. Although this is a straightforward application of the calculation technique, we think that it is interesting. However, both the tip and the substrate surface may be damaged in a contact mode, and the method to evaluate the tip in a noncontact mode should be developed. In this case, the macroscopic region of the AFM system—a large cluster model—must be considered as mentioned above. Larger models are also necessary to treat not only perfect periodic surfaces but also nonperiodic surfaces including defects and impurities. The theoretical method to include such effects of the AFM system is now being developed, and will appear in a future work.

ACKNOWLEDGMENTS

The authors would like to thank Dr. Katsuyoshi Kobayashi for many constructive suggestions. This work is partially supported by Grant-in-Aid from the Ministry of Education, Science and Culture of Japan. The numerical calculations were performed by HITAC S-3800 at the Computer Center of the University of Tokyo.

[1]G. Binnig, C. F. Quate, and Ch. Gerber, Phys. Rev. Lett. **56**, 930 (1986).
[2]D. Rugar and P. Hansma, Phys. Today **43** (10), 23 (1990).
[3]G. Binnig, Ch. Gerber, E. Stoll, T. R. Albrecht, and C. F. Quate, Europhys. Lett. **3**, 1281 (1987).
[4]O. Marti, B. Drake, and P. K. Hansma, Appl. Phys. Lett. **51**, 484 (1987).
[5]O. Marti, B. Drake, S. Gould, and P. K. Hansma, J. Vac. Sci. Technol. A **6**, 287 (1987).
[6]T. R. Albrecht and C. F. Quate, J. Appl. Phys. **62**, 2599 (1987).
[7]T. R. Albrecht and C. F. Quate, J. Vac. Sci. Technol. A **6**, 271 (1988).
[8]R. Erlandsson, G. M. McClelland, C. M. Mate, and S. Chiang, J. Vac. Sci. Technol. A **6**, 286 (1988).
[9]H.Schmidt, J. Heil, J. Wesner, and W. Grill, J. Vac. Sci. Technol. A **8**, 388 (1990).
[10]G. Meyer and N. M. Amer, Appl. Phys. Lett. **56**, 2100 (1990).
[11]E. Meyer, H. Henzelman, D. Brodbeck, G. Overney, R. Overney, L. Howald, H. Hug, T. Jung, H-R. Hidber, and H-J. Güntherrodt, J. Vac. Sci. Technol. B **9**, 1329 (1991).
[12]B. Drake, C. B. Prater, A. L. Weisenhorn, S. A. C. Gould, T. R. Albrecht, C. F. Quate, D. S. Cannell, H. G. Hansma, and P. K. Hansma, Science **243**, 1586 (1989).
[13]H-J. Butt, E. K. Wolff, S. A. C. Gould, B. D. Northern, C. M. Peterson, and P. K. Hansma, J. Struct. Biology **105**, 94 (1990).
[14]T. Thundat, R. J. Warmack, D. P. Allison, L. A. Bottomley, A. J. Lourenco, and T. L. Ferrell, J. Vac. Sci. Technol. A **10**, 3272 (1991).
[15]I. P. Batra and S. Ciraci, J. Vac. Sci. Technol. A **6**, 313 (1988).
[16]S. Ciraci, A. Baratoff, and I. P. Batra, Phys. Rev. B **41**, 2763 (1990).
[17]E. Tekman and S. Ciraci, J. Phys. Condens. Matter **3**, 2613 (1991).
[18]D. Tománek, G. Overney, H. Miyazaki, S. D. Mahanti, and H-J. Güntherrodt, Phys. Rev. Lett. **63**, 876 (1989).
[19]G. Overney, W. Zhong, and D. Tománek, J. Vac. Sci. Technol. B **9**, 479 (1991).
[20]G. Overney, D. Tománek, W. Zhong, Z. Sun, H. Miyazaki, S. D. Mahanti, and H-J. Güntherrodt, J. Phys. Condens. Matter **4**, 4233 (1992).
[21]F. F. Abraham, Inder. P. Batra, and S. Ciraci, Phys. Rev. Lett. **60**, 1314 (1988).
[22]F. F. Abraham and I. P. Batra, Surf. Sci. **209**, L125 (1989).
[23]S. A. C. Gould, K. Burke, and P. K. Hansma, Phys. Rev. B

40, 5363 (1989).
[24]H. Tang, C. Joachim, and J. Devillers, Surf. Sci. **291**, 439 (1993).
[25]S. M. Paik, S. Kim, and I. K. Schuller, Phys. Rev. B **44**, 3272 (1991).
[26]W. A. Harrison, *Electronic Structure and the Properties of Solids: The Physics of the Chemical Bond* (Freeman, San Francisco, 1980), pp. 193–197.
[27]H. J. Mcskimin and W. L. Bond, Phys. Rev. **105**, 116 (1957).
[28]A. Yoshimori and Y. Kitano, J. Phys. Soc. Jpn. **2**, 352 (1956).
[29]K. Komatsu and T. Nagamiya, J. Phys. Soc. Jpn. **6**, 438 (1951).
[30]K. Komatsu, J. Phys. Soc. Jpn. **10**, 346 (1957).
[31]U. Burkert and N. L. Allinger, *Molecular Mechanics* (American Chemical Society, Washington, D.C., 1982).
[32]W. H. Press, S. A Teukolsky, W. T. Vetterling, and B. P. Flannery, *Numerical Recipes: The Art of Scientific Computing*, 2nd ed. (Cambridge Univ. Press, New York, 1992), pp. 413–418.

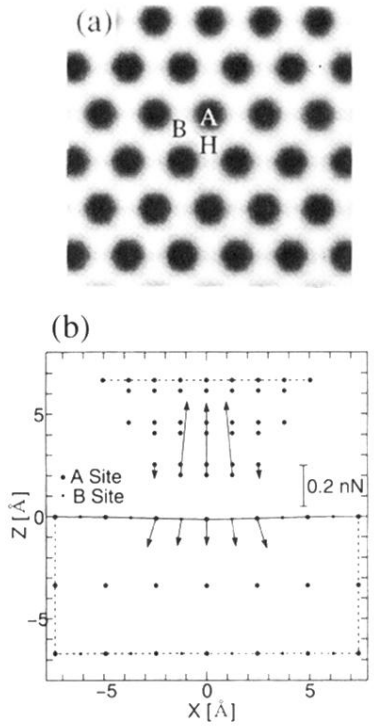

FIG. 12. (a) Constant-force image and (b) force distributions for a multiple-atom tip made up of 50 atoms. F_z is a weak repulsive force of 0.5 nN. In (a), the lateral dimensions are 13 Å × 13 Å. In (b), the multiple-atom tip is placed right above the A site. Only the x and z components of the atomic sites and the forces are shown. The larger black circles represent surface A sites or tip atoms, and the smaller black circles represent surface B sites. The broken lines denote the boundary of the cluster models.

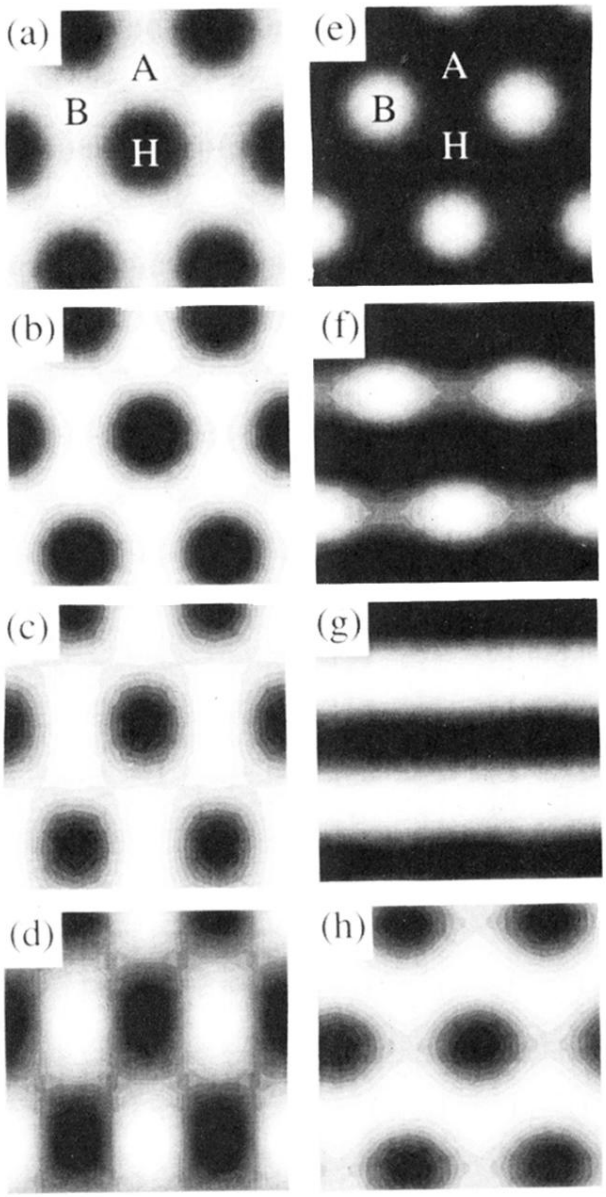

FIG. 13. (a) Constant-height image with a scanning of a single-atom tip at $z=2.3$ Å. Sum of two (a)'s in the case of $\mathbf{r}_T=$(b) $(0,d_0)$, (c) $(0,2d_0)$, (d) $(0,3d_0)$, (e) $(0,4d_0)$, (f) $(0,5d_0)$, (g) $(0,6d_0)$, and (h) $(\sqrt{3}d_0,0)$. Here $a_0=1.421$ Å and $d_0=a_0/4$. The lateral dimensions are 7 Å×7 Å.

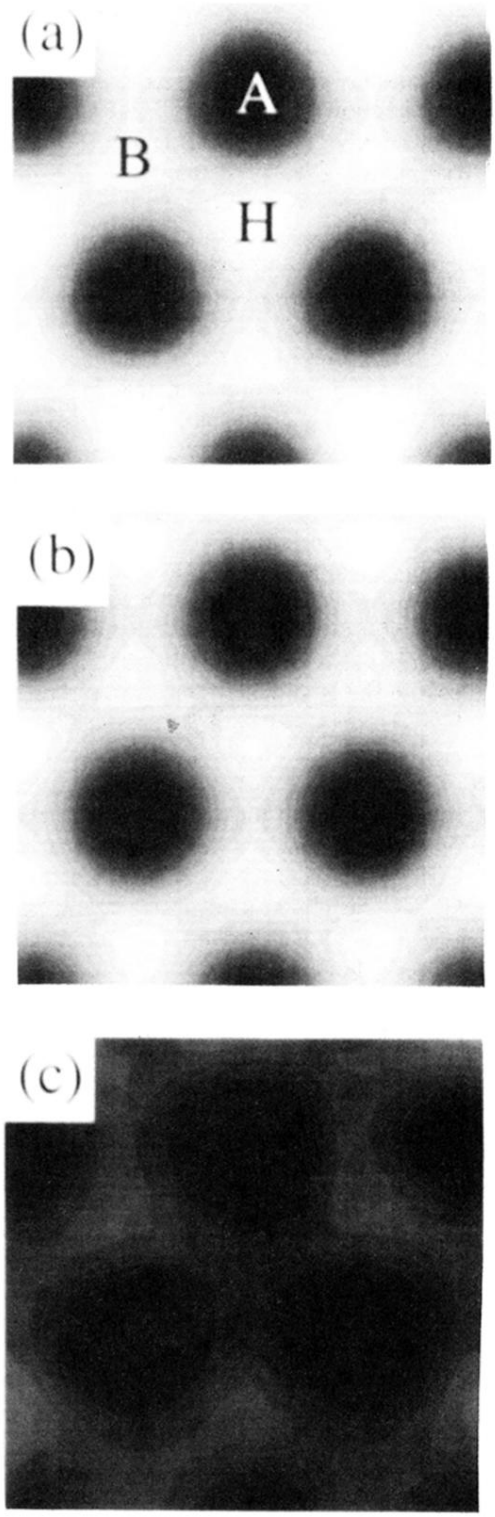

FIG. 16. The same as Fig. 15 for gray-scale expression with $N_T = 50$ and $F_z = 0.1$ nN. The lateral dimensions are 5 Å × 5 Å.

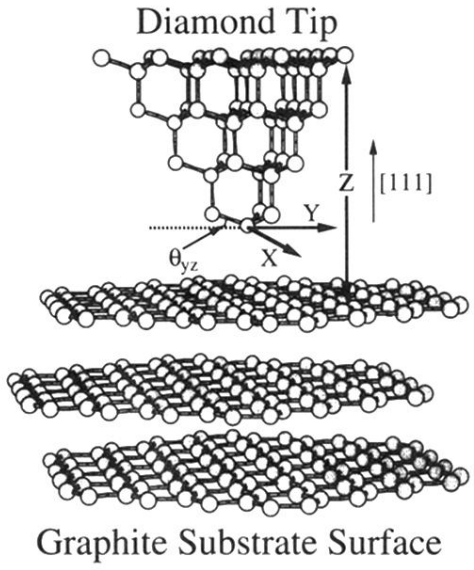

FIG. 2. The cluster model of the diamond [111] tip made up of 54 atoms and the graphite surface. Z denotes the vertical distance between the fixed basal plane of the tip and the first layer of the surface before relaxation. θ_{xy} is a tilt angle of the tip.

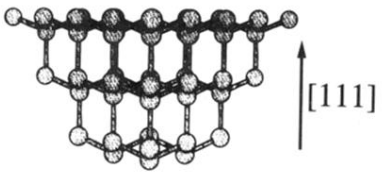

FIG. 3. Multiple-atom tip made up of 50 atoms.

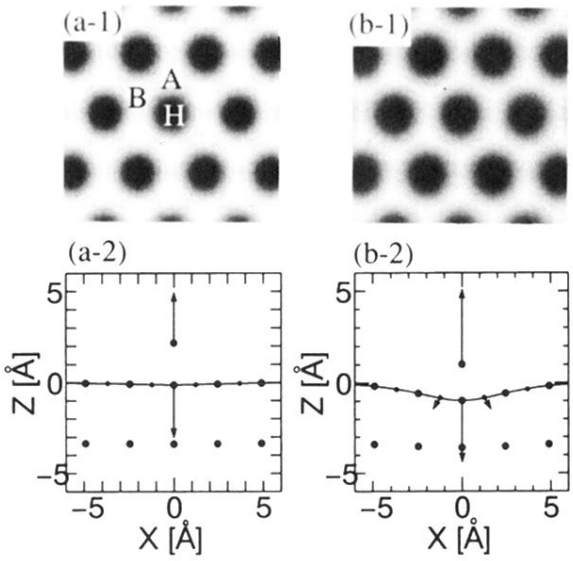

FIG. 4. Constant-force images and force distributions for a single-atom tip. The scanning force F_z is a weak repulsive force of 0.5 nN for (a-1) and (a-2), and a strong repulsive force of 5.0 nN for (b-1) and (b-2). In (a-1) and (b-1), the lateral dimensions are 8 Å×8 Å. In (a-2) and (b-2), the single-atom tip is placed right above the A site. Only the x and z components of the atomic sites and the forces are shown. The larger black circles represent surface A sites or tip atoms, and the smaller black circles represent surface B sites.

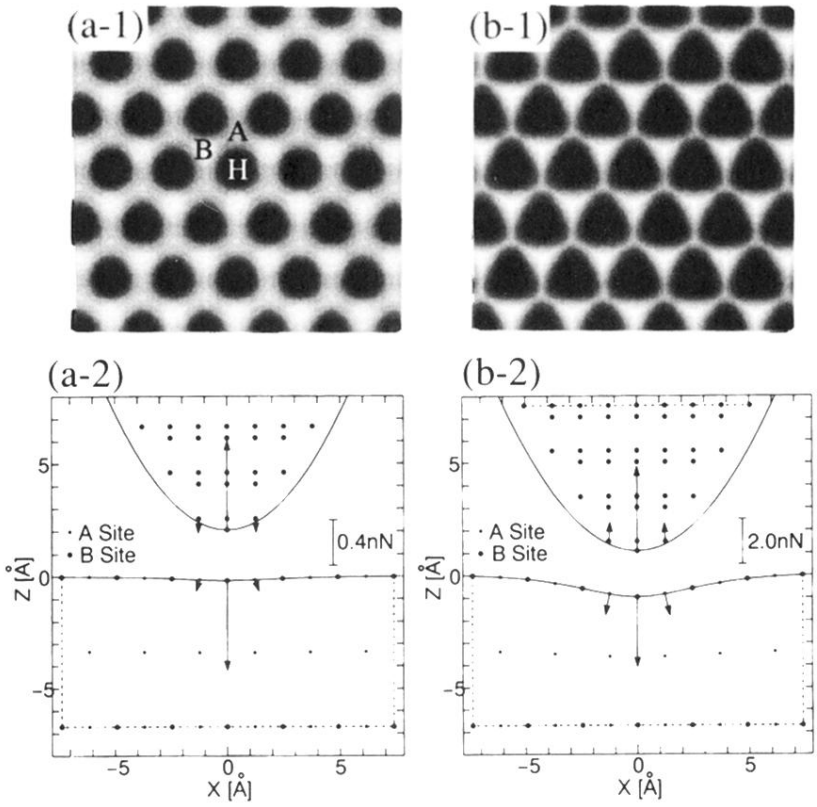

FIG. 8. The same as Fig. 4 for a multiple-atom tip made up of 54 atoms. In (a-1) and (b-1), the lateral dimensions are 13 Å×13 Å. In (a-2) and (b-2), the tip is placed right above the B site. The larger black circles represent surface B sites or tip atoms, and the smaller black circles represent surface A sites. The solid line denotes the section of the paraboloid that includes four tip apex atoms. The broken lines denote the boundary of the cluster models.

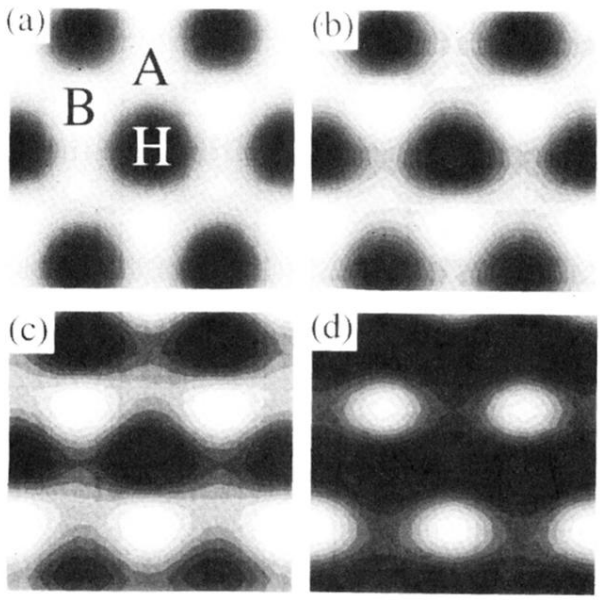

FIG. 9. Constant-force image for a multiple-atom tip made up of 54 atoms with the scanning force of 0.1 nN. The tilt angle θ_{yz} is (a) 19.5°, (b) 10°, (c) 5°, and (d) 0°. The lateral dimensions are 5 Å×5 Å.